2014-06

Production and characterization of natural rubber-Ca/P blends for biomedical purposes

Materials Science and Engineering C,Lausanne : Elsevier,v. 39, p. 29-34, June 2014
http://www.producao.usp.br/handle/BDPI/50450

Materials Science and Engineering C 39 (2014) 29–34

Contents lists available at ScienceDirect

Materials Science and Engineering C

journal homepage: www.elsevier.com/locate/msec

Production and characterization of natural rubber–Ca/P blends for biomedical purposes

R.M. Nascimento [a,b], F.L. Faita [a], D.L.S. Agostini [c], A.E. Job [c], F.E.G. Guimarães [d], I.H. Bechtold [a]

[a] Departamento de Física,Universidade Federal de Santa Catarina, 88040-900 Florianópolis, SC, Brazil
[b] Departamento de Física, Universidade Estadual Paulista, 13506-900 Rio Claro, SP, Brazil
[c] Faculdade de Ciências e Tecnologia, UNESP, Departamento de Física, Química e Biologia, CP 467, CEP 19060-080, Presidente Prudente, SP, Brazil
[d] Departamento de Física e Ciência dos Materiais,Universidade de São Paulo, Instituto de Física de São Carlos, 1356-6590, São Carlos, SP, Brazil

ARTICLE INFO

Article history:
Received 17 October 2013
Received in revised form 17 January 2014
Accepted 16 February 2014
Available online 21 February 2014

Keywords:
Natural rubber
Calcium phosphate
Biomaterial
Tissue regeneration

ABSTRACT

This study presents the development of natural rubber–Ca/P blends, as promising candidates for biomedical purposes. The specific objective was the incorporation of Ca/P into a natural rubber polymeric matrix. Ca/P crystalline phases were synthesized by the sol–gel method and the polymeric matrices were produced using natural rubber extracted from latex of the *Hevea brasiliensis*. The shape and size of natural rubber particles present in the NR membrane, as well as, the way the Ca/P powder grains aggregate in the polymeric matrix were investigated, giving information about the interactions between the Ca/P and the natural rubber particles. Confocal fluorescence scanning microscopy measurements allowed us to propose a structure where the Ca/P grains are surrounded by natural rubber particles. This structure may mediate Ca^{2+} release for tissue regeneration. The system investigated may open new horizons for development of a bandage which provides the controlled-release of biomaterials.

1. Introduction

The loss of body parts has preoccupied humanity since ancient times, stimulating the search for materials with functional surfaces that can optimize the process of tissue regeneration [1,2]. The treatment of bone defects around implants is a specific application of biomaterials in regenerative therapies, being used to isolate the wound, to prevent the invasion of epithelium cells at the site of injury and to accelerate the healing [3–8]. Considering the steps of bone regeneration, osteogenic particles can be released in a controlled manner by delivery systems to improve tissue regeneration, and the success of this process depends on the surface properties [9,10]. Such delivery systems must fulfill two specific functions: i) act as a physical barrier with sufficient strength to maintain the original functionality at the local of the lesion throughout the period in which the osteoblasts migrate into the defect; ii) induce tissue regeneration by releasing particles [11,12].

Calcium phosphates (Ca/P) can provide good biocompatibility depending on the calcium/phosphorus ratio [13,14]. The Ca/P system may present several crystalline phases, where hydroxyapatite ($Ca_{10}(PO_4)_6(OH)_2$) and the tricalcium phosphate ($Ca_3(PO_4)_2$) are the most commonly studied biomaterials and play an important role in tissue regeneration, in addition, pentacalcium octaphosphate (Ca_5P_8) has been applied as efficient reservoir of Ca and P ions in biological environments [15]. When Ca/P is precipitated in supersaturated aqueous solutions, a metastable amorphous phase forms quickly in the early stages of the reaction, being further converted to crystalline phases such as hydroxyapatite, tricalcium phosphate, and octacalcium phosphates [16].

Natural latex obtained from the *Hevea brasiliensis* tree is a colloidal system containing rubber-particles of poly-1,4-cis-isoprene (around 40% of the total latex volume) suspended in an aqueous medium. Latex can be separated into three distinct phases by centrifugation: rubber cream, serum and bottom fraction. The rubber cream is mainly composed of poly-isoprene rubber-particles, with small portions of *Hevein* proteins (Hev. b1 and Hev. b3, with low allergenicity) and phospholipids [17,18]. The serum phase contains different types of compounds, including carbohydrates, several proteins, amino acids and enzymes. Finally, the bottom fraction contains a high portion of monomers and metal ions [19,20].

Natural rubber (NR), obtained from the rubber cream, is emerging as a renewable, low-cost and biocompatible polymer [21,22] due to its low allergenicity, being employed as transdermal drug delivery systems where the NR is the controlling layer membrane [23,24]. Latex membranes have been used to promote the activity of bone regeneration through the Guided Bone Regeneration (GBR) model system by incorporating bone morphogenetic proteins on NR membranes acting as protein delivery system [25–28]. In this context, it is possible to combine the NR characteristics as a physical barrier (to the epithelial cells or other components) with particles of specific functionalities, such as Ca/P, to produce a functionalized bandage.

In this work, we describe the synthesis and characterization of Ca/P particles, as well as, the development of self-sustaining membranes where these particles are physically incorporated into the NR matrix.

http://dx.doi.org/10.1016/j.msec.2014.02.019
0928-4931/

The results suggest that the Ca/P particles are surrounded by proteins/phospholipids particles in the polymeric matrix. In addition, the interactions at the NR–Ca/P interface are discussed.

2. Experimental

2.1. Materials

Calcium nitrate tetrahydrate — $Ca(NO_3)_2 \cdot 4H_2O$ (99% purity), orthophosphoric acid — H_3PO_4 (≥85 wt.% in H_2O), ethylene glycol (PA, 99.8% purity), methyl alcohol (methanol — 99.5%, PA), ammonium hydroxide (PA-ACS) and chloroform (PA) were purchased from Sigma-Aldrich®. All the chemical products were used as received. NR was obtained from the natural latex extracted from different rubber trees (RRIM 600 clone) in Indiana City, São Paulo State, Brazil.

2.2. Synthesis and physicochemical characterization of the Ca/P powder

The Ca/P was synthesized by the sol–gel method using as precursors the calcium nitrate tetrahydrate and orthophosphoric acid in the proportion of 80:20 wt.%. The precursors were dissolved in 15 mL of a methanol:ethylene glycol solution (2:1 ratio) and maintained under magnetic stirring and ambient conditions during 1 h to produce the sol solution. The obtained product was submitted to aging, drying and annealing in three steps: i) 24 h at 50 °C under constant magnetic stirring, this procedure resulted in an opaque and viscose gel; ii) the gel was poured into ceramic dishes and dried during 1 h at 100 °C, then grounded to powder with a mortar and pestle; and iii) the resultant powder was annealed during 1 h at 700 °C and stored under ambient conditions for the future analyses. The structural, morphological and chemical properties of the Ca/P powder were investigated using X-ray diffraction (XRD) with Rietveld analysis, scanning electron microscopy (SEM) and energy-dispersive X-ray spectroscopy (EDS).

The XRD pattern was recorded on a PANalytical X'Pert PRO Multi-Purpose Diffractometer, using Cu-Kα radiation (λ = 0.15418 nm), operating at 45 kV and 40 mA and equipped with the X'Celerator detector. The measurement was carried out at 2θ angles ranging from 10° to 110° with a scan step size of 0.033° using the Bragg–Brentano (θ–2θ) geometry. Rietveld analysis [29] was performed from the complete XRD pattern using the X'Pert HighScore Plus software (version 2.2b of PANalytical, Netherlands) and the starting structural models were based on the information given in the Inorganic Crystal Structure Database (ICSD) [30]. The structural refinement by the Rietveld method allowed the determination of the main phase fractions. SEM images and EDS (X-ray from Kα energy line emission) spectra were performed with a JEOLJSM-6390LV SEM microscope (under 15 kV typical tension acceleration) equipped with a NORAN X-ray Micro-analysis System Six. ImageJ® free software was used to determine the particle size distribution from the SEM images.

2.3. NR solution and membrane production

The collected latex from the rubber trees was stabilized in ammonium hydroxide at 2% (volume) and submitted to centrifugation using a Cientec — CT 5000R centrifuge at 6000 rpm at a temperature of 4 °C for 90 min. This centrifugation process allowed the separation of the rubber cream phase fraction as previously reported [31]. The rubber cream was dried over night in an oven at 60 °C and dissolved in chloroform at a concentration of 30 mg/mL. The pure NR membrane was produced by casting the NR solution in Petri dishes followed by thermal annealing during 6 h at 45 °C in an oven. The final thickness of the membrane was measured with a digital micrometer, to be around 200 μm. A complete study about the morphological properties of NR membranes was recently reported [31].

2.4. Production of NR:Ca/P blend

The Ca/P powder was dispersed in chloroform, at a concentration of 0.1 mg/mL, and submitted to sonication during 30 min. After this procedure, the Ca/P solution was mixed with the NR solution (described in Section 2.3) in the ratio NR:Ca/P of 9:1 considering the weight of the solids and then submitted to magnetic stirring during 20 min. Finally, the NR–Ca/P blend membrane was produced by casting the NR–Ca/P solution in Petri dishes followed by thermal annealing during 6 h at 45 °C in an oven. The final thickness of NR–Ca/P blend membrane was also around 200 μm, checked with a digital micrometer.

2.5. Characterization of the membranes

The mechanical properties were investigated on both membranes by dynamic mechanical analyses (DMA) using a TA Instruments Analyzer, model DMA-Q800, in single cantilever mode. Stress–strain curves were obtained at a temperature of 30 °C with a strain rate of 2 $mm \cdot min^{-1}$ using a fixed frequency of 1 Hz. Five samples of each membrane were submitted to DMA measurements and the mean elastic modulus (E) or Young's modulus of each sample was obtained using the equation:

$$E = \frac{F/A_0}{\Delta L/L_0} = \frac{\sigma}{\varepsilon}, \quad (1)$$

where F is the force applied to the sample, ΔL is the length variation, A_0 and L_0 are the original cross-sectional area and length of the object, respectively. Therefore, σ is the tensile stress (F/A_0) and ε corresponds to extensional strain ($\Delta L/L_0$).

The incorporation of the Ca/P powder into the NR membrane was verified by EDS (chemical color mapping) measurements. The shape and size of the NR-particles (composed of proteins/phospholipids) present in the pure NR membrane and the interactions of the Ca/P powder with the polymeric matrix and/or NR-particles of the NR–Ca/P blend membrane were investigated using a Carl Zeiss LSM 780 confocal laser scanning microscope equipped with a multi-line, diode laser of 405 nm, 6 mW and 20 MHz. Moreover, a water-immersion objective (63× magnification) with the software Zen 2010 Light Edition was used for image acquisition.

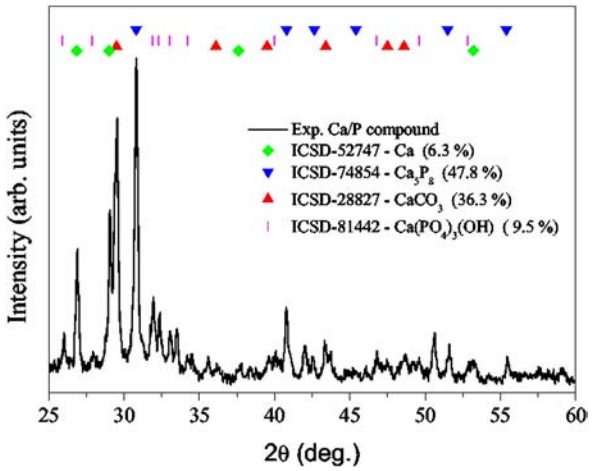

Fig. 1. XRD pattern obtained for the Ca/P powder with the identification of the main intense peaks and the estimated phase fractions by Rietveld method using the HighScore Plus® software.

3. Results and discussion

Fig. 1 shows the XRD pattern obtained for the Ca/P powder as synthesized, where crystalline phases were identified and attributed to monoclinic Ca_5P_8 (ICSD card #74854), trigonal $CaCO_3$ (ICSD card #28827) and two hexagonal $Ca(PO_4)_3OH$ (ICSD card #81442) and Ca (ICSD card #52747) phases. The Rietveld method was applied to estimate the crystalline contribution of each main phases and the majority phase fractions were: Ca_5P_8 (47.8 wt.%), $CaCO_3$ (36.3 wt.%), $Ca(PO_4)_3OH$ (9.5 wt.%) and Ca (6.3 wt.%). The final adjusted lattice parameters remained very close to those reported on the ICSD cards, indicating that the synthesis and thermal annealing processes provided a compound with reduced strain–stress lattice defects. Amorphous and crystalline samples with structural defects are structurally and chemically metastable. The properties of metastable samples can be altered by small rates of energy and/or due to aging, thus samples with reduced structural defects are desired to obtain crystalline samples stable for longer periods. Atoms located at the boundaries of the interstices and surfaces of the grains do not contribute coherently in order to satisfy the Bragg's law and therefore the XRD is not able to measure the interfacial component. In addition, the amorphous and interfacial component atoms may act as a reservoir of Ca^{2+} ions.

In the biological environment, some of these phases, such as $Ca(PO_4)_3OH$, can promote the optimization of tissue regeneration by creating a gradient of cell proliferation. The Ca/P can also present different densities and porosities due to each specific polymorph phase and/or the mixing of different Ca/P phases. Moreover, mixing distinct Ca/P polymorph phases allows different levels of degradation, caused by dissolution, which is dependent on the solubility of the material, pH and temperature. The physical disintegration into smaller particles can also occur due to biological interactions. In this process, Ca^{2+} ions may be released into the environment and the proportion of calcium and phosphorous altered [11,32].

Fig. 2 shows the SEM micrographs, the graphs resulting from the EDS measurement and the particles size distribution analyses. Fig. 2(a) shows the SEM image of the Ca/P powder as synthesized, where the graphs (I) and (II) show the histogram of the particles size distribution (centered at 13 μm) and the EDS spectrum of this image, respectively.

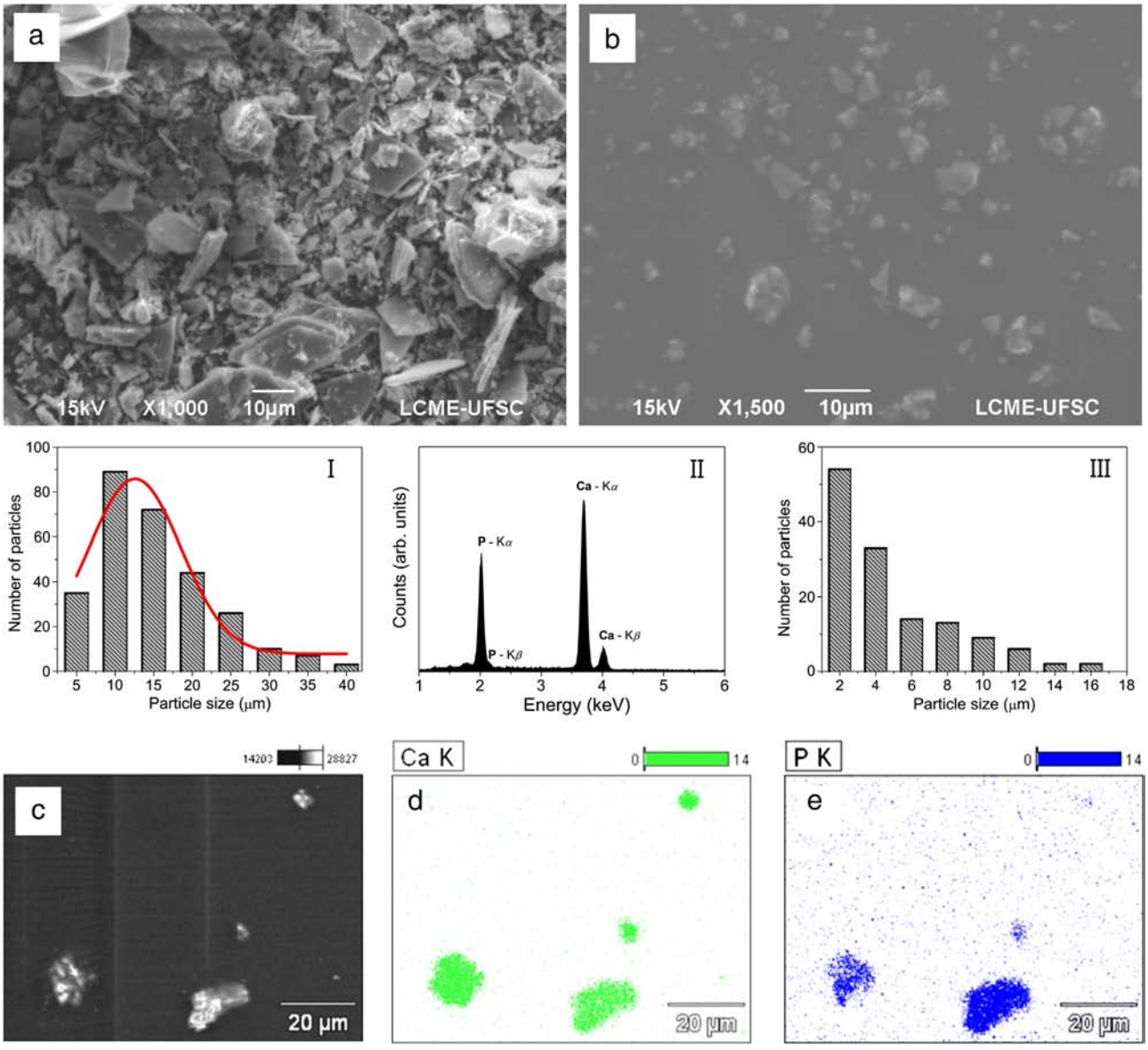

Fig. 2. SEM micrographs of the Ca/P powder as synthesized (a) and casted after dispersion and sonication in chloroform (b). Graphs I and II show the particle size histogram and EDS spectrum for the SEM image (a), respectively. Graph III shows the particle size histogram obtained for the SEM image (b). (c) represents the SEM image of the NR–Ca/P blend membrane and its EDS chemical color map of Ca and P in (d) and (e), respectively.

The EDS analysis showed a Ca/P ratio of 1.67. This value coincides with the range of Ca/P ratios typical of biological processes (0.5 to 2.0) [33]. Fig. 2(b) shows the Ca/P powder after dispersion in chloroform, sonication and casting on an NR membrane as substrate, while the new size distribution is shown in the graph (III). It can be observed that the dispersion of Ca/P particle sizes is considerably reduced, ranging from 2 to 16 μm, being predominantly under 5 μm. Fig. 2(c) shows the SEM image of the Ca/P particles incorporated into the latex membrane, and Fig. 2(d) and (e) shows its EDS chemical color map for Ca and P, respectively. These results confirm the presence of Ca and P in the observed particles and the presence of these particles homogeneously distributed in the membrane.

In order to design controlled-release systems using bioactive particles like Ca/P, a detailed understanding of the carrier properties is required. The latex membranes demonstrated good flexibility and mechanical resistance, which is an important characteristic for surgical manipulation. However, in this study, the priority was to investigate the constituents of the Ca/P–NR membranes. Concerning the NR obtained from the rubber cream phase of the latex, models in the literature describe the presence of rubber particles formed by a core–shell structure comprised of a hydrophobic core (isoprene molecules) surrounded by a mixed layer of proteins (84%) and phospholipids (16%) with around 20 nm thick [34,35]. The maximum diameter reported for these sphere-like structures is around 5 μm. In addition, these negatively-charged proteins control the colloidal stability of the latex, favoring several other factors, such as the adsorption of ions at the surface of the rubber particles [34].

From the DMA measurements we obtained elastic modules of 3.8 ± 0.1 MPa and 3.9 ± 0.1 MPa for the pure NR and NR–Ca/P blend membranes, respectively. Thus, the mechanical properties of the membranes are not affected by the Ca/P doping, which is desired for biomedical applications. The low elastic modulus is because the membranes are not vulcanized.

The produced NR membranes were investigated by confocal fluorescent scanning microscopy and well-defined spherical rubber particles with diameters ranging between 1 and 5 μm were observed. Fig. 3(a) shows the luminescence micrograph of a particle with a diameter of around 4 μm. It is important to emphasize that this image was obtained without additional dye doping for contrast. In Fig. 3(a), blue and green regions of emission can be seen throughout the particle surface, resulting in the broadband spectrum presented in Fig. 3(d). Gaussian deconvolutions were applied to the emission spectra and two contributions were estimated at maximum wavelengths of 492 nm and 559 nm (dotted line) for a single NR particle (P1) and 484 nm and 536 nm (dashed line) for NR–Ca/P (P2). These two specific emission bands can be attributed to the emission associated with two distinct structures of the tryptophan present in the proteins of the NR particles. The structural conformation of proteins has been studied [36], but in this case, our hypothesis is that solvent can change some aromatic ring chains during the process of dispersion. On the other hand, the presence of

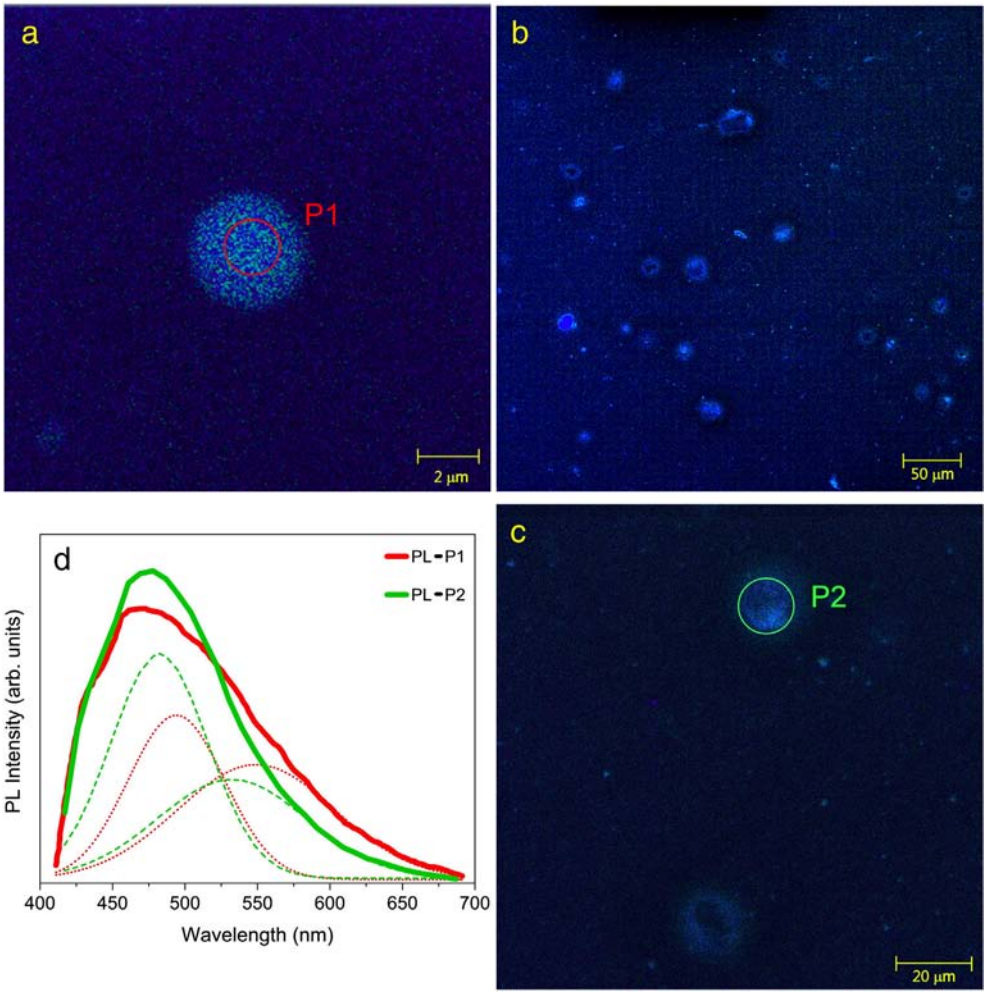

Fig. 3. Confocal luminescence micrographs of a single rubber particle captured from the unblended NR membrane (a); and the agglomerates in the NR–Ca/P blend samples (b) and (c). (d) Luminescence spectra of the P1 and P2 regions. The dashed and dotted lines are the Gaussian deconvolutions of the emission spectra. (For interpretation of the references to color in this figure legend, the reader is referred to the web version of this article.)

Ca/P particles could weakly interact with natural rubber compounds mainly modifying only the structure of the proteins which is supposed to shift the emission bands evaluated from the NR–Ca/P composites.

Fig. 3(b) shows the confocal fluorescent micrograph for the NR–Ca/P membrane, where large agglomerates with sizes of up to 30 μm can be clearly seen. In addition, the agglomerates with a focal plane at the center of the particles display an emissive border with a non-emissive core. Fig. 3(c) shows two agglomerates in detail, one with a non-luminescent asymmetric center. The emission spectrum of the P2 region is very similar to that obtained for the single rubber particle in Fig. 3(a), region P1. Moreover, we tested by same confocal microscopy measurements the Ca/P particles dispersed in a poly(methyl methacrylate) (PMMA) polymeric matrix and any emission was observed under the same experimental conditions.

By relating the two emission bands of the tryptophans present in the proteins, the analysis of Fig. 3(a) suggests a random and homogeneous distribution of these components over the NR particle embedded in the bulk of the polymeric matrix. In contradiction with previous studies reported in the literature, where models for the NR particles have been proposed, considering the proteins and phospholipids having a heterogeneous distribution, with protein/phospholipid agglomerates on the NR particle surface [34,37].

The NR particles show a resultant negative charge at around -56.7 ± 0.7 mV, as verified by zeta potential analysis, this result is in close agreement with values previously reported for a latex solution at a pH of ~10 [38]. Ca/P grains formed by regions with crystalline phases and boundary atoms can present localized positive charges due to the presence of Ca^{2+} on the surface of the grains. Thus, when in solution, these boundary atoms can promote electrostatic attraction due to the opposite charges of the NR particles and the Ca/P grains on the surface. In addition, during their diffusion to the polymeric matrix the Ca^{2+} ions can migrate around the NR particles and promote a small degree of calcification. This calcification around NR particles has been previously observed and described in the literature [39]. Multivalent cations and/or anions (e.g., Ca^{2+} and PO^{4-}) and NR latex anionic proteins could regulate their stability with this calcification [40]. Ca^{2+} ions have the ability to bridge negatively charged entities, such as carboxylate groups and phosphate groups in charged and zwitterionic lipid species, or negative charges in the NR. Calcium is a fusogenic agent and has a profound effect on the adsorption of vesicles [41]. Calcium ions do not only participate in the screening of the charges, thereby modifying the electrostatic interactions, but they also directly interact with surfaces and lipids present in the NR [42]. These considerations may explain the increasing size of agglomerates observed in the NR–Ca/P membranes (see Fig. 3(b) and (c)). Moreover, surface interactions between the NR particles and the Ca/P grains may also occur and contribute to the formation of NR–Ca/P agglomerates. A schematic representation showing the possible configuration of the NR–Ca/P agglomerates is proposed in Fig. 4(a) and a schematic representation of the NR particles adapted from Ref. [34] is presented in Fig. 4(b). It is important to note that the non-spherical shape of the agglomerates, together with the dimensions of the non-emitting center and the luminescent shell of Fig. 3(b) and (c) is consistent with the proposed representation in Fig. 4(a).

4. Conclusions

In summary, the sol–gel process was used to produce Ca/P micrograins with multi-crystalline phases, including the monoclinic Ca_5P_8 and the hexagonal $Ca(PO_4)_3OH$. The percentage contribution of each phase was estimated by applying the Rietveld method to XRD measurements, where the major phase fractions obtained were: Ca_5P_8 (47.8 wt.%), $CaCO_3$ (36.3 wt.%), $Ca(PO_4)_3OH$ (9.5 wt.%) and Ca (6.3 wt.%). The chemical ratio between Ca and P was 1.67, as verified by EDS analysis, this value being within the bioactivity range. The spherical shape (with ~4 μm of diameter) and homogeneous distribution of the proteins and phospholipids on the shell of the NR particles were observed by luminescent confocal microscopy. The interaction of the NR particles with the Ca/P grains was confirmed via confocal micrographs, supporting the proposed structure, i.e., that the Ca/P grains are surrounded by NR particles, as shown in Fig. 4(a). This aspect represents the novelty of this study. This system may open new horizons in relation to its use as a biomaterial for application in tissue regeneration. The results presented herein are the first step toward obtaining a bandage which promotes the controlled-release of biomaterials. The degradation of natural rubber, the release of Ca^{2+} ions in a simulated body fluid and the biocompatibility of the material with tissue regeneration are currently under investigation.

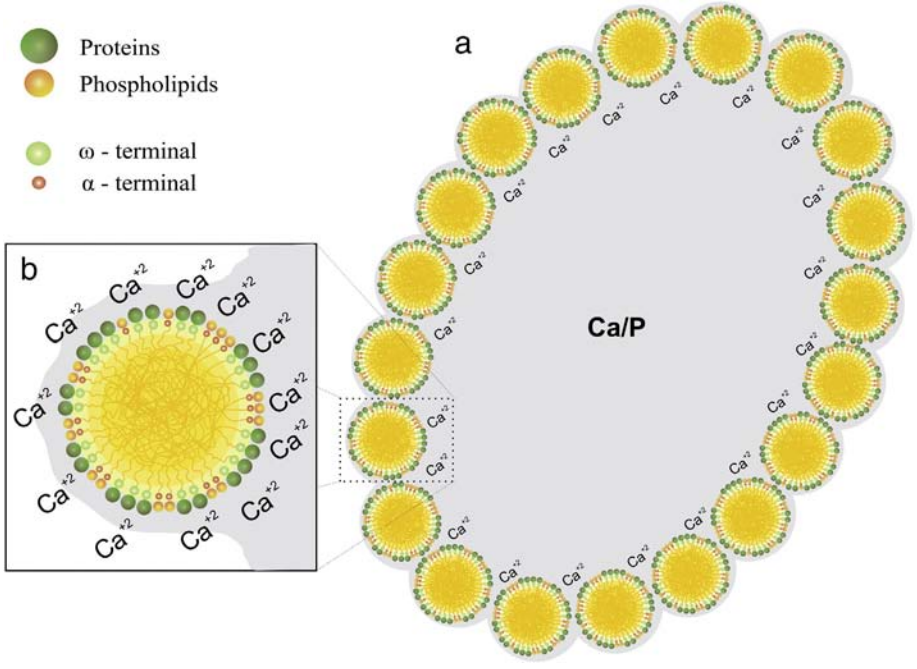

Fig. 4. (a) Suggested schematic representation of an NR–Ca/P agglomerate. (b) Detailed description of the proposed structural organization of the NR particles adapted from Ref. [34], where the proteins and ω-terminals, as well as the phospholipids and α-terminals, with their connections, are represented.

Acknowledgments

The authors are grateful to the Brazilian governmental agencies CNPq (project #555100/2010-3), CAPES (project PNPD/2583/2011), INCT/INEO and NanoBiomed for financial support and the Central Laboratory of Electron Microscopy (LCME–UFSC) by SEM and EDS facilities. The XRD experiment was carried out in the Laboratório de Difração de Raios-X (LDRX-CFM/UFSC).

References

[1] M.M. Stevens, Mater. Today 11 (2008) 18–25.
[2] P. Broz, Knovel (Firm), RSC Nanoscience and Nanotechnology, 9, Royal Society of Chemistry, Cambridge, UK, 2010, p. 1, (online resource, xv, 372 pp.).
[3] S.Y. Shin, H.N. Park, K.H. Kim, M.H. Lee, Y.S. Choi, Y.J. Park, Y.M. Lee, Y. Ku, I.C. Rhyu, S.B. Han, S.J. Lee, C.P. Chung, J. Periodontol. 76 (2005) 1778–1784.
[4] N.S. Satarkar, J.Z. Hilt, Acta Biomater. 4 (2008) 11–16.
[5] N.S. Satarkar, D. Biswal, J.Z. Hilt, Soft Matter 6 (2010) 2364–2371.
[6] W.F.P. Neves-Junior, M. Ferreira, M.C.O. Alves, C.F.O. Graeff, M. Mulato, J. Coutinho-Netto, M.S. Bernardes, Braz. J. Phys. 36 (2006) 586–591.
[7] A. Sculean, G.C. Chiantella, P. Windisch, N.B. Arweiler, M. Brecx, I. Gera, J. Clin. Periodontol. 32 (2005) 720–724.
[8] M. Kikuchi, Y. Koyama, T. Yamada, Y. Imamura, T. Okada, N. Shirahama, K. Akita, K. Takakuda, J. Tanaka, Biomaterials 25 (2004) 5979–5986.
[9] G.R. Owen, J. Jackson, B. Chehroudi, H. Burt, D.M. Brunette, Biomaterials 26 (2005) 7447–7456.
[10] S. Liao, W. Wang, M. Uo, S. Ohkawa, T. Akasaka, K. Tamura, F.Z. Cui, F. Watari, Biomaterials 26 (2005) 7564–7571.
[11] H.H.K. Xu, M.D. Weir, L.M. Sun, Dent. Mater. 25 (2009) 535–542.
[12] R.D. Herculano, A.A.A. de Queiroz, A. Kinoshita, O.N. Oliveira, C.F.O. Graeff, Mater. Sci. Eng. C Mater. 31 (2011) 272–275.
[13] H.H. Xu, J.L. Moreau, L. Sun, L.C. Chow, Dent. Mater. 27 (2011) 762–769.
[14] W. Thein-Han, J. Liu, H.H. Xu, Dent. Mater. 28 (2012) 1059–1070.
[15] C. Hadenfeldl, F. Barlels, Z. Anorg. Allg. Chem. 620 (1994) 1247–1252.
[16] A.H. Aparecida, M.V.L. Fook, M.L.d. Santos, A.C. Guastaldi, Quim. Nova 30 (2007) 892–896.
[17] J.M. Rolland, R.E. O'Hehir, Clin. Exp. Allergy 38 (2008) 898–912.
[18] A.M. Smith, H.S. Amin, R.E. Biagini, R.G. Hamilton, S.A. Arif, H.Y. Yeang, D.I. Bernstein, Clin. Exp. Allergy 37 (2007) 1349–1356.
[19] M.M. Rippel, C. Leite, L.-T. Lee, F. Galembeck, Colloid Polym. Sci. 283 (2004) 570–574.
[20] D.L.S. Agostini, C.J.L. Constantino, A.E. Job, J. Therm. Anal. Calorim. 91 (2008) 703–707.
[21] F. Mrué, J.C. Netto, R. Ceneviva, J.J. Lachat, J.A. Thomazini, H. Tambelini, Mater. Res. 7 (2004) 277–283.
[22] C.A. Balabanian, J. Coutinho-Netto, T.L. Lamano-Carvalho, S.A. Lacerda, L.G. Brentegani, J. Oral Sci. 48 (2006) 201–205.
[23] E. Abraham, P.A. Elbi, B. Deepa, P. Jyotishkumar, L.A. Pothen, S.S. Narine, S. Thomas, Polym. Degrad. Stab. 97 (2012) 2378–2387.
[24] W. Pichayakorn, J. Suksaeree, P. Boonme, W. Taweepreda, T. Amnuaikit, G.C. Ritthidej, Chem. Eng. Res. Des. 91 (2013) 520–529.
[25] R.D. Herculano, C.P. Silva, C. Ereno, S.A.C. Guimaraes, A. Kinoshita, C.F.D. Graeff, Mater Res. Ibero-Am. J. 12 (2009) 253–256.
[26] C. Ereno, S.A.C. Guimaraes, S. Pasetto, R.D. Herculano, C.P. Silva, C.F.O. Graeff, O. Tavano, O. Baffa, A. Kinoshita, J. Biomed. Mater. Res. A 95A (2010) 932–939.
[27] M.A.C. Frade, I.B. Cursi, F.F. Andrade, J. Coutinho-Netto, F.M. Barbetta, N.T. Foss, Med. Cutan. Iber. Lat. Am. 32 (2004) 157–162.
[28] M. Ferreira, R.J. Mendonca, J. Coutinho-Netto, M. Mulato, Braz. J. Phys. 39 (2009) 564–569.
[29] H.M. Rietveld, J. Appl. Crystallogr. 2 (1969) 65–71.
[30] Inorganic Crystal Structure Database (ICSD), Gmelin-Institut für Anorganische Chemie and Fachinformationszentrum, FIZ, Karlsruhe, 2007.
[31] F.L. Faita, M.E.R. Dotto, L.G. França, F.C. Cabrera, A.E. Job, I.H. Bechtold, Eur. Polym. J. 50 (2014) 249–254.
[32] W.I. Abdel-Fattah, F.M. Reicha, T.A. Elkhooly, Biomed. Mater. 3 (2008) 034121.
[33] R.Z. LeGeros, Monogr. Oral Sci. 15 (1991) 1–201.
[34] K. Nawamawat, J.T. Sakdapipanich, C.C. Ho, Y. Ma, J. Song, J.G. Vancso, Colloids Surf. A Physicochem. Eng. Asp. 390 (2011) 157–166.
[35] R. Wititsuwannakul, K. Rukseree, K. Kanokwiroon, D. Wititsuwannakul, Phytochemistry 69 (2008) 1111–1118.
[36] L. Bateman, Natural Rubber Producers' Research Association, The Chemistry and Physics of Rubber-like Substances, , Maclaren, London, 1963.
[37] K. Berthelot, S. Lecomte, Y. Estevez, V. Zhendre, S. Henry, J. Thevenot, E.J. Dufourc, I.D. Alves, F. Peruch, Biochim. Biophys. Acta (2013), http://dx.doi.org/10.1016/j.bbamem.2013.1008.1025.
[38] J. Sansatsadeekul, J. Sakdapipanich, P. Rojruthai, J. Biosci. Bioeng. 111 (2011) 628–634.
[39] M.M. Rippel, C.A. Leite, L.T. Lee, F. Galembeck, J. Colloid Interface Sci. 288 (2005) 449–456.
[40] B.Y. Ha, Phys. Rev. E. 64 (2001).
[41] R.P. Richter, R. Berat, A.R. Brisson, Langmuir 22 (2006) 3497–3505.
[42] I. Reviakine, A. Simon, A. Brisson, Langmuir 16 (2000) 1473–1477.